Cell PRESS
Neuron
Article

Olfactory Coding with Patterns of Response Latencies

Stephan Junek,[1,2,3,4,5,*] Eugen Kludt,[1,5] Fred Wolf,[4,5,6] and Detlev Schild[1,2,3,4,5]
[1]Department of Neurophysiology and Cellular Biophysics
[2]DFG Research Center for Molecular Physiology of the Brain (CMPB)
University of Göttingen, Humboldtallee 23, 37073 Göttingen, Germany
[3]DFG Excellence Cluster 171
[4]Bernstein Focus Neurotechnology Göttingen
[5]Bernstein Center for Computational Neuroscience
Bunsenstrasse 10, 37073 Göttingen, Germany
[6]Max Planck Institute for Dynamics and Self-Organization and, Faculty of Physics, Göttingen University
*Correspondence: sjunek@gwdg.de
DOI 10.1016/j.neuron.2010.08.005

SUMMARY

The encoding of odors by spatiotemporal patterns of mitral/tufted (M/T) cells in the vertebrate olfactory bulb has been discussed controversially. Motivated by temporal constraints from behavioral studies, we investigated the information contained in odor-evoked first-spike latencies. Using simultaneous recordings of dozens of M/T cells with a high temporal resolution and quantitative ensemble correlation techniques, we show that latency patterns, and in particular latency *rank* patterns, are highly odor specific and reproducible. They reliably predict the odor identity as well as the odor concentration on a single-trial basis and on short timescales—in fact, more reliably than patterns of firing rates. Furthermore, we show that latency ranks exhibit a better reproducibility at the level of M/T cells than in olfactory receptor neurons. Our results suggest that the latency patterns of M/T cells contain all the information higher brain centers need to identify odors and their concentrations.

INTRODUCTION

At the level of the olfactory bulb (OB) odor information is contained in the spike patterns of mitral/tufted (M/T) cells. Today it is generally assumed that in addition to the identity of the activated M/T cells, the temporal patterns of their responses are important for olfactory coding (Friedrich and Laurent, 2001; Laurent et al., 2001; Schaefer and Margrie, 2007). However, it is still unclear as to which aspects of these spatiotemporal patterns contain the odor-specific information that is subsequently decoded by the OB's target areas. M/T cell activities were reported to be dynamically modulated over a timespan of seconds, which has motivated models that are based on transient correlations among M/T cells (Friedrich and Laurent, 2001). On the other hand, behavioral studies in vertebrates show that odor discrimination and recognition can be accomplished within 500 ms or even less depending on the task and the species (Abraham et al., 2004; Laing, 1986; Rinberg et al., 2006; Slotnick, 2007; Uchida and Mainen, 2003; Wesson et al., 2008). Attention has thus been directed toward activity features on shorter timescales, such as instantaneous firing rates, the average firing phase, and response latencies (Bathellier et al., 2008; Lehmkuhle et al., 2006; Schaefer and Margrie, 2007). The latter have been shown to be important coding parameters in the visual (Burr and Ross, 1979; Gawne et al., 1996; Gollisch and Meister, 2008), the somatosensory (Johansson and Birznieks, 2004; Panzeri et al., 2001; Petersen et al., 2002), and the auditory (Carr and Konishi, 1990; Heil, 1997) system. In the olfactory system, odor- and concentration-dependent latencies have been described at the level of both olfactory receptor neurons (ORNs) (Carey et al., 2009; Getchell and Shepherd, 1978; Gomez and Atema, 1996; Spors et al., 2006; Verhagen et al., 2007) and M/T cells (Bathellier et al., 2008; Cang and Isaacson, 2003; Hopfield, 1995; Kauer and Shepherd, 1977; Margrie and Schaefer, 2003; Scott, 2006; Spors and Grinvald, 2002; Wellis et al., 1989). However, a potential role for odor coding has been discussed controversially (Bathellier et al., 2008; Schaefer and Margrie, 2007).

In order to elucidate the specificity and reproducibility of odor response latencies, one has to meet two crucial requirements: (1) M/T cell responses need to be measured at a sufficiently high temporal resolution and simultaneously, since only simultaneous recordings can reveal the relative response latencies that may contain the odor-specific information. (2) The similarity of the latency patterns of the M/T cell population under investigation has to be quantified in order to assess the patterns' reproducibility and specificity under different experimental conditions. Since studies satisfying both requirements are lacking, the role of response latencies in olfactory coding has remained unclear thus far.

We solve this issue here by using a fast confocal line illumination microscope (Junek et al., 2009) and ensemble correlation techniques. The resulting evidence reveals that latency vectors of M/T cells are reproducible and odor specific. They accurately predict the odor identity on a single-trial basis and on short

timescales. Latency patterns thus appear to contain the information higher brain centers would need to identify odors and their concentrations.

RESULTS

M/T Cells Show Odor-Dependent Response Latencies

We recorded the odor-evoked M/T cell activities in nose-brain preparations (Czesnik et al., 2003) of larval *Xenopus laevis* using the cell-permeable calcium-sensitive dye fluo-4 AM. Using a custom-built confocal line-illumination microscope (Junek et al., 2009; Figure S1A), we were able to simultaneously record the activities of dozens of OB neurons at a rate of 100 Hz (Figures 1 and S1B). Amino acids were used as stimuli, as they have been shown to be behaviorally relevant odors for tadpoles (Kiseleva, 1995). Odorants were applied to the nose through a funnel applicator using an electrical pipette triggered to the beginning of the fast acquisition period (Figures 1A and S1B). From the fluorescence time course of each responsive M/T cell, we determined the time point of its response latency, i.e., the time point of the first odor-evoked spike relative to the trigger of the application system (Figures 1B and 1C).

Figure 1E shows exemplary responses of four M/T cells to repeated applications of the amino acid arginine (50 μM). The response latencies of the neurons (indicated by vertical lines) are similar for the three applications. Furthermore, the order in which the neurons start to respond to the stimulus, i.e., the latency order, is unchanged. In Figure 1F, the regions of interest (ROIs) assigned to 20 M/T cells from the same slice preparation are superimposed on the raw fluorescence image and color coded for their response latencies in the trials used for Figure 1E. The response latencies of the neurons are very reproducible. Figures 1G and 1H show the response latencies of the same neurons to stimulations with the amino acid methionine (50 μM). While the latencies are also reproducible for repeated applications of methionine, they differ markedly from the latencies observed during the application of arginine. This suggests that M/T cells respond reproducibly with latencies that are specific for the applied odor. In the following, we quantify the specificity and reproducibility of the M/T cell latency patterns.

Simultaneous Recordings Are Required for Obtaining Odor-Specific Patterns

In order to choose an appropriate analysis approach, we wanted to know whether the simultaneously acquired across-neuron latencies capture information that cannot be assessed by pooling successive recordings from individual neurons. Figure 2A shows 39 latencies $L(s,a,c)$ recorded in 13 cells ($c = 1, 2, \ldots, 13$) upon three applications ($a = 1, 2, 3$) of the stimulus methionine (s = met). There are two fundamentally different ways of looking at these latencies. First, the ensemble statistics view, where simultaneously recorded latencies are viewed as ensembles (blue, green, and red curve in Figure 2A), i.e., as latency vectors $L_{\mathrm{met},a}(c)$ (see Experimental Procedures for nomenclature). Alternatively, the trial statistics view, where we have sequences of three latencies $L_{\mathrm{met},c}(a)$ for each cell (i.e., columns of data points in Figure 2A).

Obviously, a stimulus response as a whole does not occur at a predefined, fixed time. It rather includes a certain trial-dependent shift (in agreement with odor-evoked responses recorded in the turtle OB; Lam et al., 2003), which appears to be similar in different cells. It comprises the odor delivery (see Figure 1A) as well as a network component. In fact, in the trial statistics view, the latencies of successive trials using the same stimulus s of the m^{th} cell, $L_{s,c_m}(a)$, tend to be highly correlated to the corresponding latencies of the n^{th} cell, $L_{s,c_n}(a)$ (Figure 2B).

The trial-dependent shift of an odor response can easily be described, in the ensemble statistics view, as the trial's latency ensemble mean,

$$\overline{L_{\mathrm{met}}}(a) = \langle L_{\mathrm{met},a}(c) \rangle_c = \frac{1}{13} \sum_{c=1}^{13} L_{\mathrm{met},a}(c)$$

(horizontal lines in Figure 2A). As every latency comprises an odor-specific latency and the trial's ensemble mean, the latter has to be known (measured) for each trial and subtracted to yield the odor-specific information (Figure 2C). This is obviously a rather crucial point for the design of experiments on odor coding. For example, as the trials' ensemble means are intrinsically unknown in measurements carried out sequentially over trials cell after cell, it is impossible to derive reliable odor-specific patterns from such measurements.

Quantification of Latency Vector Similarity

We thus decided to quantify the similarity of *latency vectors* (rather than the latencies of individual neurons), on a single-trial basis and independent of an external time frame. A "latency vector" consists thereby of the (simultaneously recorded) latencies after which each M/T cell fired its first spike upon stimulus application. Two measures were used for this quantification: the correlation coefficient (CC), which measures the degree to which two latency vectors are linearly related to each other (Figure S2, left column), and Kendall's rank correlation coefficient (RCC, Kendall and Gibbons, 1990), which assesses the similarity of the *order* of the neurons' latencies (Figure S2, right column).

The left panel of Figure 2D shows the distribution of CCs using pairs of latency vectors in response to eight applications of methionine (response latencies of the 20 neurons shown in Figure 1D). The distribution has a peak at 0.9, the lowest values being 0.75. Randomizing the application order for each neuron—thereby simulating recordings of individual cells pooled from successive trials—shifts the distribution toward smaller values, with a peak at 0.6 (left panel of Figure 2E). To further illustrate the strong reproducibility of the measured latency patterns, we simulated a system in which latencies do not contain any stimulus-related information by artificially creating random sequences of "latencies." The left panel of Figure 2F shows the distribution of the CCs for these sequences, which is symmetric around 0. The right panels of Figures 2D–2F show the corresponding distributions of the RCC, which exhibit a similar sensitivity to a randomization of the application order (Figure 2E). Both measures thus capture the information contained in the timing of the parallel M/T cell output.

Latency Vectors Are Highly Reproducible and Depend on Odor Identity

Using these tools, we investigated the reproducibility and odor specificity of M/T cell latency vectors by stimulating the

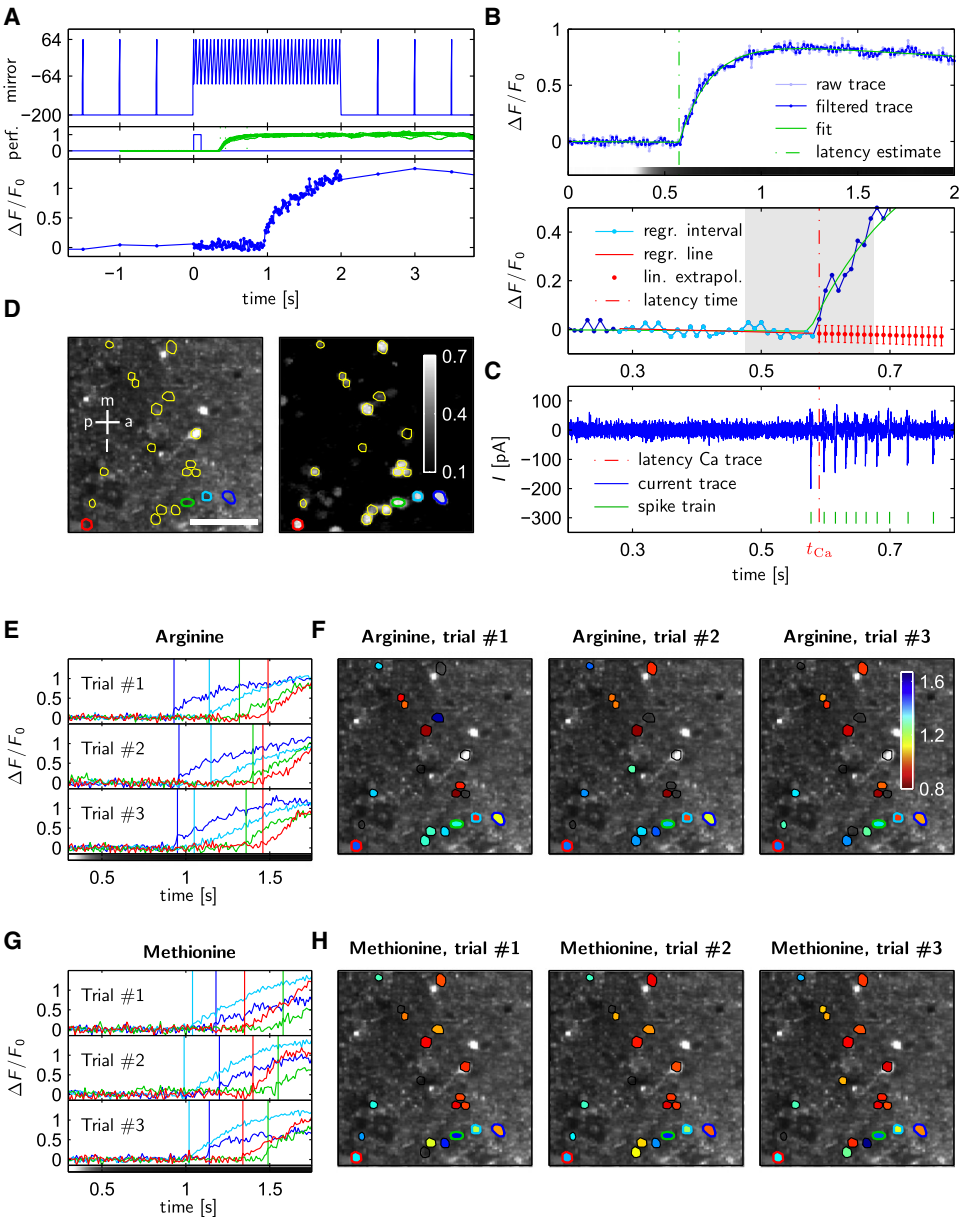

Figure 1. Investigation of Odor-Evoked Response Latencies in M/T Cell Ensembles by Fast Confocal $[Ca^{2+}]_i$ Imaging

(A) The fast image acquisition (100 Hz) was flanked by slower acquisition (2 Hz) to monitor levels of spontaneous activity and the late phase of the response (top). A trigger (middle, blue trace) started the odor application, which was very reproducible as quantified using fluorescein as "odor" and an acquisition frequency of 400 Hz (middle, green traces, ten applications, standard deviation at 50% of maximum intensity ~19 ms). In comparison, the across-trial variability of neuronal response latencies had a median of 84 ms in our experiments. Exemplary response of a M/T cell (bottom).

(B) The determination of the response latency from the Ca^{2+} trace consists of three steps (see Experimental Procedures for details). 1, smoothing (top panel, dark blue line); 2, estimating the latency from a global fit (top panel, green line); 3, determination of the precise latency based on a local linear regression (bottom panel, red line; vertical red bars indicate linear prediction intervals).

(C) Simultaneously to the Ca^{2+} trace shown in (B), the electrical activity of the cell was recorded (on-cell voltage clamp; blue, current trace; green vertical lines, extracted spike train). The difference between the Ca^{2+} latency t_{Ca} and the first spike latency t_{spike1} was 18.4 ± 8.3 ms (ten traces from three neurons). While the mean is not relevant to our analysis (it represents a general temporal offset for all neurons), the standard deviation indicates the maximum accuracy expected for an interframe interval of 10 ms. In all cases (10/10) t_{Ca} was larger than t_{spike1}, and in 9/10 cases t_{Ca} was smaller than the time point of the second spike. Therefore, in no case did we encounter a false early detection, and in almost all cases was the detected rise in the Ca^{2+} trace unambiguously the result of a single action potential. Therefore, the term "response latency" (as detected from the Ca^{2+} trace using our algorithm) can be used synonymously with the term "first spike latency."

(D) Mean projection over time (left) and "autocorrelation map" (right) of a fluo4-stained OB slice preparation. The autocorrelation map facilitated the selection of somata that responded reproducibly to certain odors (correlation coefficients as gray scale colormap). Indicated are 20 somata responding to the amino acids arginine and methionine. Scale bar, 50 μm.

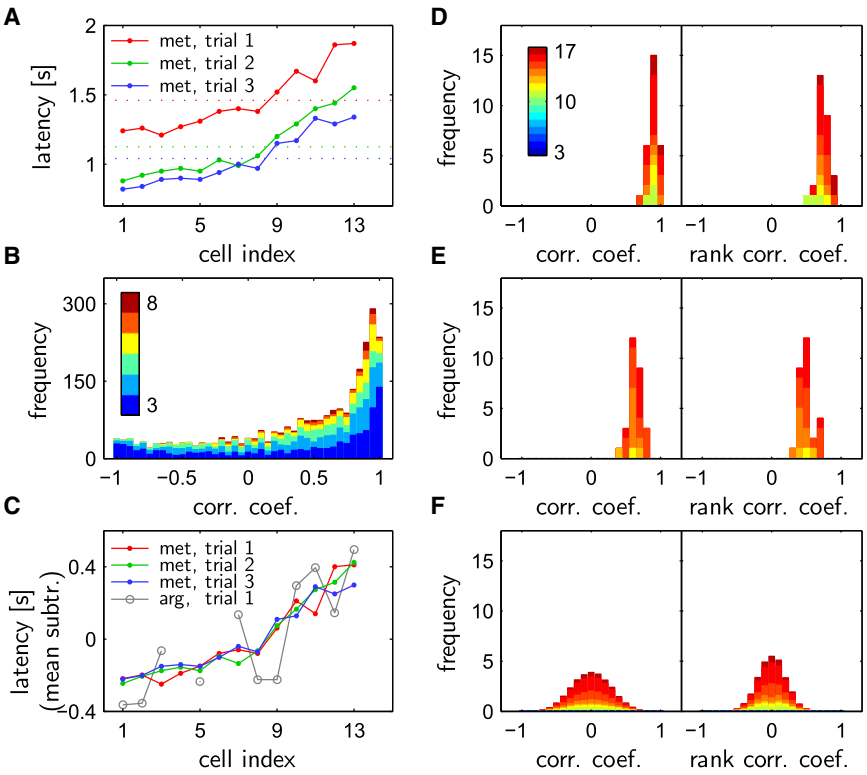

Figure 2. Simultaneous Recordings Are Required to Obtain Odor-Specific Patterns

(A) Response latencies of 13 neurons during three applications of methionine. The across-trial latencies of each neuron vary significantly, but this variability appears to be very similar for all the (simultaneously recorded) cells. The latencies can thus be decomposed into a trial-specific shift common to the complete network, which can be described by the ensemble's mean latency (horizontal lines), and a cell-specific latency that varies only slightly across trials (see also C).

(B) Correlation of response latencies for pairs of cells across applications of a given stimulus. For each stimulus S and each cell pair (c_m, c_n) the correlation coefficient of the latency vectors $L_{s,c_m}(a)$ and $L_{s,c_n}(a)$ across applications a of this stimulus was computed (247 neurons in 14 slices, various stimuli). The distribution of these coefficients shows a strong correlation between the response latencies of the M/T cells within a slice, indicating that the neurons' latencies covary across trials. Colors indicate number of trials.

(C) Subtracting the ensemble's mean latency for each trial removes the trial-dependent shift and extracts the odor-specific latency pattern (same data as A). These patterns are highly reproducible for successive applications of the same stimulus. The gray line shows the neurons' latencies in response to an application of arginine, thereby demonstrating the odor-specificity of the neurons' latencies.

(D) Distribution of CCs and RCCs (left and right panel, respectively) of latency vectors $L_{S,A_i}(c)$,$L_{S,A_j}(c)$ for all application pairs (A_i, A_j) of eight applications of methionine (same preparation as shown in Figure 1). The distributions are centered at 0.9 and 0.7, respectively, thereby indicating a high degree of reproducibility. Different colors represent different numbers of neurons underlying the calculated CC or RCC (see color bar).

(E) When randomizing the application order prior to calculating the CCs (left) and RCCs (right), the resulting distributions are significantly shifted to smaller values.

(F) Distribution of CCs (left) and RCCs (right) for artificial randomly generated "latency sequences" (using the same lengths of latency vectors as in E). These distributions are centered at 0, thereby emphasizing the high degree of reproducibility of the measured latency (rank) vectors used for E.

See also Figure S3.

olfactory system with a number of amino acids (arginine, methionine, and phenylalanine, each 50 μM). These amino acids are known to activate highly overlapping populations of M/T cells (Manzini et al., 2007) and form therefore, despite their small number, a suitable set of odors to investigate olfactory coding based on temporal structures of response patterns. For a given slice preparation we calculated the CCs of latency vectors $L_{S_i,A_m}(c)$ and $L_{S_j,A_n}(c)$ for all possible pairs of trials ((S_i, A_m), (S_j, A_n)) and sorted them with respect to stimulus pairs S_i/S_j (i.e., Arg/Arg, Arg/Met, etc.; see Experimental Procedures for nomenclature). The distributions of CCs for each stimulus pair are shown in Figure 3A. Comparing different applications of the same odor (histograms on the diagonal) yields distributions in the range of 0.7 to 0.9. This shows that the latency vectors are highly reproducible for all stimuli. Comparing, on the other hand, responses to different odors yields distributions centered on smaller values (the off-diagonal distributions in Figure 3A). The distributions are approximately Gaussian-shaped with an odor-pair-specific mean value which varied only slightly from slice to slice, i.e., CCs pooled from various slices (n = 6) give similar distributions (Figure S3A). To facilitate the evaluation of pattern similarity for trials using either identical or different stimuli, the CCs from six slices were sorted and pooled, and bootstrap analyses were performed (Figure 3B). The distributions of CCs from pairs of trials using either identical or disparate stimuli are distributed around 0.7 and 0.35, respectively. Similar results were obtained when quantifying latency vector similarities using the RCC (Figures S3C and S3D). Hence,

(E) Responses and response latencies (vertical lines) of four somata (indicated by the same colors as in D) to three applications ("trials") of arginine.

(F) Response latencies of the 20 neurons shown in (D) in the three arginine trials used for (E) depicted as color-coded overlay over the fluorescence OB image (see color bar).

(G) Responses of the four somata indicated in color in (D) to three applications of methionine and their response latencies, which differ from those shown in (E).

(H) Response latencies of the 20 neurons shown in (D) in the three methionine trials used for (G) depicted as color-coded overlay over the fluorescence OB image (same colorbar as F).

See also Figure S1.

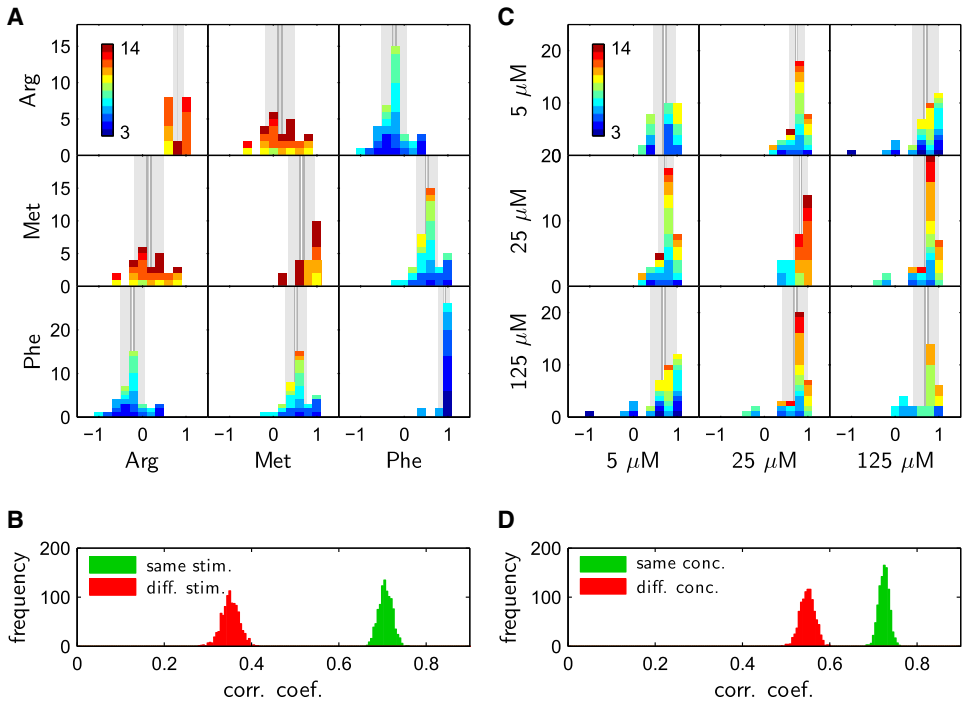

Figure 3. Latency Patterns of M/T Cells Are Highly Reproducible, Odor Specific, and Depend Only Weakly on Odor Concentration

(A) Distributions of CCs for odor stimulation with different amino acids. Shown is a symmetrical "matrix" of CC distributions, one panel for each pairing of stimuli (data from a single slice). Different colors represent different numbers of neurons underlying the calculated CC (see color bar). The histograms along the diagonal are distributed close to one. This indicates a high degree of reproducibility of latency vectors during repeated applications of the same stimulus. The off-diagonal histograms represent the latency vectors' odor specificity. Compared to the distributions on the diagonal, they are strongly shifted toward lower values. This shift appears to be odor-pair specific. The white lines indicate the positions of the weighted mean, the light gray and gray bars the width of the weighted standard deviation and standard error of the mean, respectively.

(B) CCs of six slice preparations were pooled and sorted into two categories (comparing identical or different odors). The displayed distributions are the result of bootstrap analyses and confirm that the latency vectors are highly reproducible and odor specific.

(C) Distributions of CCs for stimulations with different concentrations of the same odor (arginine). In all histograms the distributions are close to one, with only minor differences between the on- and off-diagonal histograms.

(D) Bootstrap analyses performed on results pooled from eight slice preparations show a small dependence of latency vectors on the odor's concentration. This dependence is however much smaller than the dependence on the odor identity shown in (B).

See also Figure S3.

latency vectors of M/T cell populations are odor specific and highly reproducible. This is not only true for individual odorants (such as amino acids), it also holds for complex mixtures of odorants (Figures S3G and S3H).

Latency Vectors Depend Only Weakly on Odor Concentration

Given the odor specificity of latency vectors, it was necessary to consider a possible interference by odor concentration. To test the concentration dependence of latency vectors, we quantified the similarity of the M/T cell latency vectors for applications of arginine at different concentrations (5 μM, 25 μM, 125 μM). The concentrations used cover the dynamic range of effective stimuli (Czesnik et al., 2003). Figure 3C shows the distributions of CCs of latency vectors for all pairs of stimulus concentrations. In contrast to Figure 3A, both the diagonal and the off-diagonal distributions are roughly in the same range (0.7–0.9), thereby showing that latency vectors are largely independent of the odor's concentration. To obtain a more accurate assessment of the concentration dependence, we performed a bootstrap analysis on the results pooled from eight slice preparations (Figure 3D). The resulting distributions are significantly closer than those shown in Figure 3B. The small—yet systematic—dependence of latency vectors on odor concentration (which is also apparent when using the RCC; Figures S3C and S3D) thus does not appear to compromise the potential role of latency vectors in coding odor identity.

Latency Vectors Reliably Predict Odor Identity and Odor Concentration

How accurately can a stimulus be predicted based on the latency vector of a single trial? To address this question, we assumed that the brain tries to match latency vectors against template vectors formed during previous exposures. Here we constructed such a template $L_S^{\text{templ}}(c)$ from the latency vectors $L_{S,A_1}(c)$, $L_{S,A_2}(c)$, … from all applications A_i of stimulus S (see Experimental Procedures). Every recorded latency vector $L_{S_{\text{trial}},A}(c)$ was then assigned to its most similar template $L_{S_{\text{predict}}}^{\text{templ}}(c)$, and the

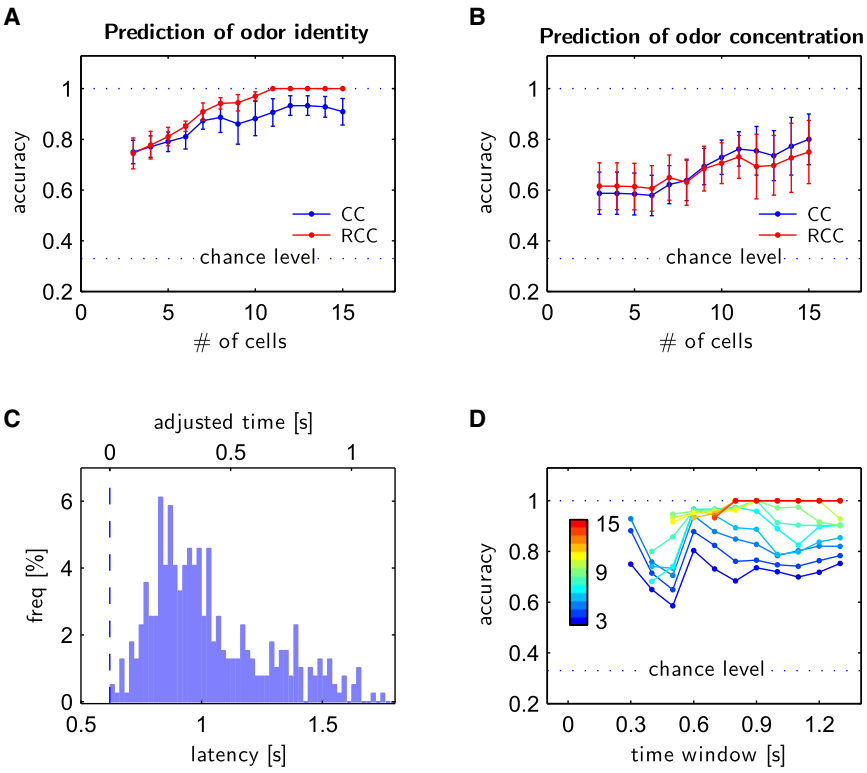

Figure 4. Latency Vectors Predict Odor Identity and Odor Concentration Fast and Reliably

(A) Accuracy of odor prediction based on latency vectors using the CC and the RCC (mean ± SEM, from six slice preparations, same data as Figure 3B; x axis: minimum length of latency vectors considered). The RCC is a better predictor for odor identity than the CC. The accuracy reaches 100%, if the latencies of more than ten neurons are known. The CC only reaches accuracies of about 90% even for long latency vectors. The chance level is 33%.

(B) Accuracy of prediction of odor concentration using the CC and the RCC (mean ± SEM, from eight slice preparations, same data as Figure 3D). Despite the weak concentration dependence of the latency vector, the concentration can be predicted with an accuracy of almost 80%. RCC and CC perform comparably well.

(C) Distribution of mean response latencies of 247 cells in 14 slices using a variety of stimuli (averaged for each cell across applications of the same stimulus). The shortest latency of 0.62 s (measured relative to the stimulus trigger) is used as the $t_0 = 0$ s for the time-resolved classification test shown in (D).

(D) The accuracy of odor prediction based on latency vectors was determined for time windows ranging from 0.1 to 1.4 s. While the accuracy strongly depends on the number of neurons, it is virtually independent of the time window's width. Already for time windows as short as 400 ms an accuracy of about 80% is possible with sufficiently long latency vectors.

stimulus $S_{predict}$ of this template (the "predicted stimulus" of this trial) was matched against the trial's actual stimulus S_{trial}. We were thus able to evaluate whether latency vectors contain sufficient information to reliably identify the applied odor. Figure 4A shows the success rate of this classification test as a function of the vector's length (i.e., the number of cells) for experiments using different amino acids (top panel, same data as Figure 3B). The RCC proved to be an excellent predictor of odor identity and consistently yielded a success rate of 100% if latencies of more than ten neurons were available, while the CC did not exceed an accuracy of 90% even for patterns consisting of up to 15 neurons. This demonstrates that the order of latencies is a slightly better predictor for the odor's identity than the actual time differences between the neurons' latencies. Next, we performed the classification test on the data using different concentrations of the same amino acid (Figure 4B, same data as Figure 3D). Despite the strong similarity of latency vectors (Figures 3C and 3D), the predictions using either the CC or the RCC still reached an accuracy of about 80% at a 33% chance level. Notably, the majority of false predictions (84%) resulted from mistaking "neighboring" concentrations, thus demonstrating that only rather dissimilar concentrations can be distinguished on the basis of latency vectors. The classification tests thus show that the pattern of response latencies is a very reliable indicator of odor identity and can even predict odor concentration with a certain accuracy.

Latency Vectors Reliably Predict Odor Identity on Short Timescales

The results shown in Figures 4A and 4B are based on latencies observed in a 2 s recording period. As we were particularly interested in odor coding on short timescales, we analyzed the prediction accuracy for shorter time windows. Since it was not possible to precisely determine the time the odor reached the receptor neurons, we estimated this time by the shortest M/T cell latency measured in any slice preparation (Figure 4C). Starting from this time point, we performed the classification test on time windows ranging from 0.1 to 1.4 s. As the RCC proved to be a better predictor of odor identity than the CC (Figure 4A), we performed this analysis using the RCC. The prediction accuracy as a function of the time window's width is shown in Figure 4D as a series of curves, the different colors indicating the length of the latency vector (i.e., the number of latencies considered). Interestingly, while the accuracy strongly depends on the vector length (as observed already in Figure 4A), it is almost completely independent of the time window's length (all plots are approximately parallel to the abscissa). For time windows of 300–400 ms the odor can be predicted with an accuracy of about 70%–80%, while for time windows of 500 ms a prediction accuracy of 95% can be achieved when the latencies of at least nine neurons are known. This demonstrates that even on short time scales, latency vectors provide a reliable indicator of odor identity.

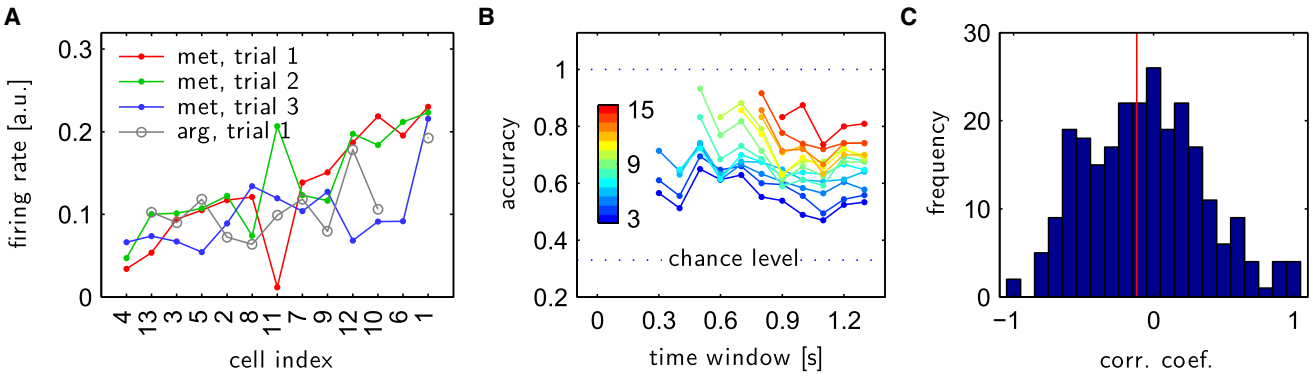

Figure 5. Patterns of Firing Rates Predict Odor Identity Less Accurately than Latency Vectors

(A) Shown are the firing rate vectors computed from the recordings used for the latency vectors shown in Figure 2C (three trials of methionine application and one trial of arginine application). Cells are sorted according to the trial-averaged firing rates (only methionine trials). The corresponding cell index of Figure 2 is indicated by labels along the x axis. Cells 4 and 6 are not responding to arginine. Compared to the latency vectors, the firing rate vectors exhibit a lower degree of reproducibility and odor specificity.

(B) Accuracy of odor prediction based on vectors of instantaneous mean firing rates for various vector lengths and time windows (same data as used for Figure 4D). The prediction accuracy is significantly lower compared to the use of latency vectors and does not reach 100%, not even for long vectors and long time windows.

(C) Distribution of correlation coefficients between latencies and instantaneous firing rates (based on a total of 2635 value pairs from 14 slice preparations using a variety of odors and concentrations). Latencies and firing rates are largely uncorrelated with a slight bias toward negative values (red line indicates mean value of −0.12).

See also Figure S4.

Firing Rate Vectors Predict Odor Identity Less Accurately than Latency Vectors

Firing rates have often been suggested as a means of coding olfactory information in the OB (Bathellier et al., 2008; Friedrich and Laurent, 2001; Lehmkuhle et al., 2006). Recently, there have been successful attempts to determine changes in firing rates from the intensity fluctuations of calcium-sensitive dyes (Lin et al., 2007; Moreaux and Laurent, 2008; Yaksi and Friedrich, 2006). Using the method by Yaksi and Friedrich, we could show that the reconstruction efficiency of M/T cell firing rates is in our model system as high as in the original publication (Figure S4A). Vectors of odor-evoked instantaneous firing rates showed a strongly reduced reproducibility and specificity when compared to latency vectors (Figure 5A, based on the same data as Figure 2C). In order to quantitatively evaluate a potential role of firing rate vectors for predictive coding, we performed the time-resolved classification test (as used for latency vectors, see Figure 4D) on patterns of instantaneous M/T cell firing rates (Figure 5B). Similarly to the predictions based on latency vectors, the prediction accuracy of firing rates strongly depends on the number of cells, whereas it depends only weakly on the length of the time window. However, vectors of firing rates are consistently less accurate predictors of odor identity than latencies vectors. They never reach 100% accuracy, not even for long time windows and long vectors. For the prediction of odor concentration, a similar discrepancy between accuracies based on latencies or firing rates was found for time windows longer than 0.7 s (Figures S4B and S4C). These observations raise the question whether firing rates carry information independent from latencies, or whether firing rates contain redundant albeit less reliable information. Figure 5C shows that firing rates and latencies are essentially uncorrelated, thus indicating that latencies and firing rates might carry independent information. This is in line with previous reports both for glomerular (Spors et al., 2006) and M/T cell (Margrie and Schaefer, 2003) responses.

Latency Vectors in Olfactory Receptor Neurons

The existence of odor-specific latencies at the level of M/T cells raises the question of their origin. While odor-specific latency vectors have been qualitatively described at the level of ORNs (Spors et al., 2006), we quantitatively compared properties of latency vectors of ORNs and M/T cells. By electroporating ORNs with fluo-4 dextran, we were able to selectively record from the axon terminals of ORNs in olfactory glomeruli (Figures 6A, 6B, and S5). Figure 6C shows 14 ROIs superimposed on a cluster of amino-acid-sensitive glomeruli, with the colors of the ROI center and circumference indicating the latencies upon arginine and methionine application, respectively (averaged over eight trials each). These averaged latencies constitute the first rough confirmation of odor-specific latencies in *Xenopus* ORNs. In order to quantify the specificity and reproducibility of these patterns, we calculated the CCs for eight applications of each arginine, methionine, and phenylalanine (Figure 6D). Similarly to the results obtained for M/T cells, the distributions along the diagonal are significantly shifted toward larger values when compared to the off-diagonal histograms. This was confirmed by pooling the results of four slice preparations and sorting the CCs according to comparisons of identical versus different odors (Figure 6E).

In order to compare the reproducibility of latency vectors in ORNs and M/T cells, we performed bootstrap analyses on the results from four slice preparations using both the CC and the RCC as similarity measures (Figure 6F). Interestingly, the similarity of latency vectors during repeated applications of the

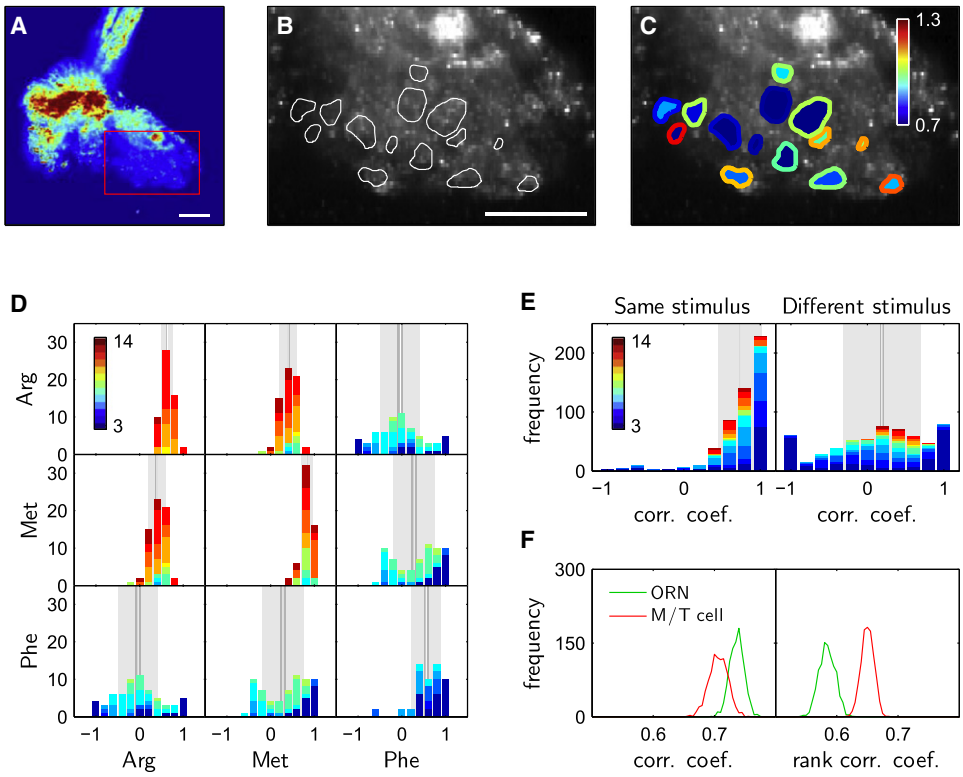

Figure 6. Rank Latency Vectors of ORNs Are Odor Specific but Less Reproducible than Those of M/T Cells

(A) Staining of presynaptic terminals of olfactory glomeruli allows to measure response latencies of ORNs. The red rectangle indicates a cluster of amino acid sensitive glomeruli that was imaged during odor application (see B). Scale bar, 50 μm.

(B) Mean projection over time of the amino acid-sensitive cluster, superimposed are 14 ROIs indicating glomeruli that responded reproducibly to the amino acids arginine and methionine. Scale bar, 50 μm.

(C) Similar display as in (B), with the color of the circumference and the center of the ROIs indicating the response latencies averaged over eight applications of arginine and methionine, respectively (see color bar). The averaged latencies indicate the existence of odor-specific latency vectors at the level of ORNs.

(D) Quantification of the odor specificity and reproducibility of latency vectors from the slice shown in (A)–(C) using the CC. The diagonal histograms are distributed around 0.7–0.9, while the off-diagonal distributions are shifted toward 0.

(E) Pooled results of four slice preparation, sorted into two categories (identical versus different stimuli).

(F) Bootstrap analyses performed on ORN and M/T cell latency vectors (green and red, respectively) using the CC and RCC (left and right panel, respectively). While the distributions of CCs are highly overlapping, the RCCs of M/T cells are shifted toward larger values compared to those of ORNs, indicating a higher degree of reproducibility of latency rank vectors at the level of M/T cells.

See also Figure S5.

same stimulus measured with the CCs is comparable at both the ORN and the M/T cell level (overlapping distributions), while RCCs show a higher degree of reproducibility in M/T cells than in ORNs.

DISCUSSION

Ensemble Coding of Olfactory Information

Today it is generally agreed that odors are encoded by activity patterns of M/T cell populations. By analyzing synchronously acquired activities of M/T cell ensembles, we were able to show that latency vectors are odor specific and highly reproducible. Most previous studies investigating spatiotemporal activity patterns, however, obtained such patterns by pooling recordings from different trials and animals (Bathellier et al., 2008; Friedrich and Laurent, 2001; Khan et al., 2008). However, this approach ignores the fact that trial-to-trial fluctuations in odor responses can be correlated across neurons, and these correlations contribute to the information content of the pattern. This might explain why a previous study concluded that mitral cell firing rates are a better predictor of odor identity than response latencies (Bathellier et al., 2008). In this study, we were able to record from a large number of neurons simultaneously, and this likely explains why we find that latencies are a better predictor of odor identity than firing rates. We found that latencies in different cells were indeed correlated across trials, which explains why latencies can form the basis of a robust odor code which is relatively insensitive to trial-to-trial variability. When we performed odor classification on the basis of firing rates using the approach of Bathellier et al. (2008), we obtained results similar to that of Bathellier et al. (Figure S5D), implying that our firing rates are not less informative than those in that study.

Our observation of latencies being better odor predictors than firing rates is paralleled by studies in the visual system (Gollisch and Meister, 2008) and is supported by studies showing that M/T cell latencies, in contrast to firing rates, vary strongly with stimulus intensity (Cang and Isaacson, 2003; Margrie and Schaefer, 2003). The presented results are further supported by previous studies based on synchronous recordings of ORN (Spors et al., 2006) and M/T cell (Spors and Grinvald, 2002) activity, which reported odor-specific and reproducible latency vectors, but lacked any quantification or classification tests.

The interpretation of our comparison between ORN and M/T cells (Figure 6F) is presently not complete, mainly because little is known about the OB's targets. Our results suggest that the sequence of events (rather than their exact timing) is more important for the receivers of the OB, whereas in the case of the primary afferents, the precise timing is more important.

Fast Odor Discrimination Requires Fast Odor Encoding

While the notion of the sense of smell as a slow sense is still correct, behavioral studies have provided quantification as to just how slow it really is. Different discrimination tasks in various species showed that around 500 ms or less are sufficient for odor recognition (Abraham et al., 2004; Laing, 1986; Rinberg et al., 2006; Slotnick, 2007; Uchida and Mainen, 2003; Wesson et al., 2008). While being much slower than the signal processing in the auditory or visual system, this is indeed much faster than previously assumed for the olfactory system. Odor coding thus needs a re-evaluation which has to comply with this timescale. The relative response latencies and the odor prediction times we observed in our experiments were in the range of a few hundred milliseconds, coinciding perfectly with the timescale reported in the discrimination studies. While the behavioral relevance of smelling amino acids is well established for tadpoles, there are no studies concerning time scales for odor discrimination in these animals. Our study provides a time frame for a minimum interval in which sufficient latency information for a reliable discrimination is contained. Additionally, our classification analysis supports the idea that a latency code is more robust than a rate code.

In agreement with our study, odor- and concentration-dependent latencies have also been observed in the olfactory bulb of breathing vertebrates (Bathellier et al., 2008; Cang and Isaacson, 2003; Margrie and Schaefer, 2003; Spors and Grinvald, 2002). Some of these species show response times significantly shorter than 500 ms (Abraham et al., 2004; Uchida and Mainen, 2003), which might be related to their ability to increase odor flux and thereby accelerate the accumulation of odor in the mucosae by sniffing. A potential link between the sniff duration and discrimination time of different species was already suggested earlier (Laing, 1986) and is supported by data obtained since (Abraham et al., 2004; Uchida and Mainen, 2003). More strikingly, it was shown in rats that response latencies strongly vary with sniff rate (Wesson et al., 2009) and flow rate (Scott, 2006). Based on this hypothesis aquatic animals would be expected to show longer discrimination times than animals that sniff air.

Interpretation of the Classification Tests

In order to capture simultaneous recordings at a high temporal resolution and in a reasonable number of trials, we used three chemically similar odorants with highly overlapping populations of activated M/T cells. The task of predicting one of these odors against the other two was relatively easy compared to real world situations. The difference in performance between firing rate patterns on the one hand and latency vectors on the other is nonetheless striking: the recognition accuracy by latency vectors "saturates" at 100% already for short time windows and short latency vectors. Latency vectors thus contain more than sufficient information for this three-odor classification test and have the potential to provide accurate information in more demanding situations. On the other hand, firing patterns produced errors even for long time windows and long vectors, and their performance would presumably worsen in more demanding situations.

We showed that if a fixed number of latencies are considered, the prediction accuracy does not depend on the time window's width. This means that early and late first spike latencies are about equally informative. In practice, of course, an observer considering a fixed number of cells will see more latencies in a long window than in a short window, and thus a long window will yield higher accuracy. It should also be noted that the OB contains significantly more M/T cells than we were able to observe in a single *z*-plane in our high-speed image acquisition experiments. The olfactory system can thus exploit much longer latency vectors than our algorithm, which thus provides a lower limit for the prediction accuracy. As the prediction accuracy was shown to depend strongly on the pattern's length while being virtually independent of the time window, even shorter times are likely to yield high prediction accuracies if long latency vectors were involved.

Effect of Odor Concentration

One of the surprising results of this study was the unexpectedly high prediction accuracy (up to 80%) for odor concentration. However, it is known that the perception of an odor can indeed depend on its concentration, as long as sufficiently different concentrations are used. Typically, the odor concentration has to be changed by one to two orders of magnitude in order to elicit a sensation of a different odor *quality* (Gross-Isseroff and Lancet, 1988; Laing et al., 2003; Wright et al., 2005), which is the range covered in our experiments. In fact, we showed that the majority of the false predictions of the odor concentration resulted from the misclassification of adjacent concentrations. Latency vectors can thus account for an odor perception that is insensitive to small yet sensitive to large changes in odor concentration.

The Role of Response Latencies in the Olfactory and Other Sensory Systems

Further support for the latency coding hypothesis comes from behavioral studies in humans (Laing et al., 1994). Individual components of odor mixtures are often detected with a slight delay, with the "faster" component frequently masking the "slower" one. By introducing a small delay in the presentation of the components, both the recognition order and the masking effect can be reversed. These phenomena can readily be explained by the latency vector coding paradigm.

Response latencies, in particular first-spike latencies, have been implicated in coding strategies in various sensory systems

such as the visual system (Burr and Ross, 1979; Gawne et al., 1996; Gollisch and Meister, 2008), the somatosensory system (Johansson and Birznieks, 2004; Panzeri et al., 2001; Petersen et al., 2002), and the auditory system (Carr and Konishi, 1990; Heil, 1997). Specifically, latencies were suggested to play a role in the fast processing of sensory information. These results are further supported by theoretical considerations showing that rate codes are significantly less efficient and slower than codes based on spike times (Thorpe et al., 2001). All these reports are in line with our observation that latency vectors are a more reliable and faster predictor of odor identity than firing rate patterns.

Rank Order Coding Using Vectors of Response Latencies

While the results using the CC or the RCC were similar in many respects, we demonstrated that the rank of the latencies is a better predictor for odor identity than the actual latency times in our system. Furthermore, the RCC appears to display a better reproducibility at the M/T cell level than the CC, which might result from processing in the OB. Rank order coding based on response latencies has previously been used to interpret biological data (Johansson and Birznieks, 2004) and has been the subject of theoretical studies (Delorme, 2003; Van Rullen and Thorpe, 2001; Thorpe et al., 2001; Thorpe and Gautrais, 1998).

Decoding of Response Latencies

The proposition of a coding scheme immediately raises the question about potential read-out mechanisms that might be employed by higher brain areas. Many of the previously proposed olfactory coding schemes use a global reference signal, the information being contained in the spike times relative to this reference (Hopfield, 1995; Laurent et al., 2001; Margrie and Schaefer, 2003). However, patterns of spike times can carry information autonomously, without relying on a global reference (Margrie and Schaefer, 2003; Schaefer and Margrie, 2007). Hopfield was one of the first to note that the piriform cortex, one of the targets of OB output, is a suitable structure for learning and decoding interneuronal time delays (Hopfield, 1995). Another biologically plausible mechanism for decoding spatio-temporal spike patterns was recently introduced as the Tempotron (Gütig and Sompolinsky, 2006). Most notably however, a simple feed-forward shunting inhibition mechanism was proposed as an efficient, flexible and robust realization for decoding latency ranks (Delorme, 2003; Thorpe et al., 2001).

Clearly, fast odor discrimination based on latency vectors by no means precludes additional coding mechanisms acting on slower timescales. Temporal response patterns over seconds might enable the sommelier to distinguish the scents of similar wines, while latency vectors might enable the antelope to recognize the predator just in time.

EXPERIMENTAL PROCEDURES

Slice Preparation and Staining of Tissue

Tadpoles of *Xenopus laevis* (stage 51–54; Nieuwkoop and Faber, 1967) were chilled in a mixture of ice and water and decapitated, as approved by the Göttingen University Committee for Ethics in Animal Experimentation. Tissue slices containing the olfactory mucosae, the olfactory nerves and the anterior two-thirds of the brain were prepared as described earlier (Manzini et al., 2002).

To stain M/T cells via bath incubation, fluo-4/AM (Molecular Probes, Karlsruhe, Germany) was dissolved in 20% Pluronic F-127 in DMSO, and then diluted in the bath solution to the final concentration (2–5 μM). Transporter-mediated destaining was avoided by adding MK571 (50 μM; Alexis Biochemicals, Lörrach, Germany) to the staining solution (Manzini et al., 2008). The slices were incubated for 30 min, followed by a postincubation period of 30 min in Ringer solution with MK571 (50 μM).

For the presynaptic glomerular imaging, ORNs were stained via electroporation as follows. The animal was anesthetized with MS-222 (0.02%, Sigma, Deisenhofen, Germany), placed on a preparation dish covered with silicon, and the caudal part of the tadpole was covered with wet cellulose tissue. Small crystals (1–10 μg) of fluo-4-dextran (Invitrogen, Karlsruhe, Germany) were placed in both nasal cavities. After the crystals dissolved, two platinum electrodes were inserted into the nasal cavities. The dye was transferred into the cells by electroporation (six pulses of 20 V and 20 ms duration). After 5 min the animal was placed back into the water. Experiments were carried out 1–2 days later.

Microscopy

Calcium imaging was carried out on a custom-built confocal line-illumination microscope described earlier (Junek et al., 2009; Figure S1A). The standard scan protocol used for investigating M/T cell responses consisted of three phases (Figure 1A): 5 s at a frame rate of 2 Hz, 2 s at 100 Hz, 5 s at 2 Hz. Synchronized to the start of the fast acquisition period, a trigger was sent to the odor application system. For the fast imaging of olfactory glomeruli, the acquisition rate was 50 Hz. The following objectives were used: 25 × LD LCI Plan-Apochromat 0.8 W and 40 × Achroplan 0.8 W (both from Zeiss, Jena, Germany). To increase the field of view without compromising temporal resolution, the images were sampled anisotropically (pixel dimensions 0.8 μm × 1.9 μm and 0.54 μm × 1.08 μm for the 25 × and 40 × objective, respectively). "Dark images" for background estimation were acquired for each experiment by closing the laser shutter and otherwise identical acquisition parameters.

Stimuli and Odor Application System

The olfactory system was stimulated with solutions containing amino acids or an extract of amphibia food (Mikrozell, Dohse Aquaristik, Bonn, Germany). The amino acids (Sigma, Deisenhofen, Germany) were dissolved in bath solution (10 mM stock) and diluted prior to the experiment to the concentrations indicated in the text. They were applied individually or as a mixture of 15 amino acids. For the solution containing food extract, 0.5 g of Spirulina algae was dissolved in 100 ml bath solution and filtered (0.5 μm pore size, Minisart, Sartorius AG, Göttingen, Germany). Odors were applied in a randomized order (six to eight applications per odor), with a minimum interstimulus interval of 1.5 min. Bath solution served as a negative control (three applications per slice).

For odor application experiments, a perfusion system described earlier was used (Manzini et al., 2002; Figure S1B). The odors were applied into the funnel without stopping the flow of the bath solution using an electronic pipette (HandyStep electronic, Brand, Wertheim, Germany) modified in order to control the outflow with an external trigger signal. The timing and reproducibility of the stimulus application was measured by adding fluorescent dye (1 μM fluorescein, Sigma, Deisenhofen, Germany) to the stimulus solution, and imaging the outflow from the tip of the applicator with a 10× objective (Zeiss, Jena, Germany) at 400 Hz. The delay was measured to be (436 ± 19) ms for 50% of the maximum concentration (n = 10 applications, mean ± SD; see Figure 1A).

Electrophysiology

Spike trains of M/T cells were recorded by on-cell voltage clamp using pipettes (8–10 MΩ input resistance) filled with Ringer solution. Traces were recorded with an EPC7 plus amplifier (Heka, Germany) using custom software for output to the amplifier and data acquisition.

Data Analysis

All data analysis was performed using custom software written in MATLAB (The MathWorks, USA).

Preparation of Data

The image data recorded by the CCD camera were transformed into

$$\Delta F/F_0 = \frac{F(t) - F_0}{F_0}$$

values after subtraction of the background. F_0 was determined pixel-wise as the mean of the intensity values of the first ten data points.

Selection of Regions of Interest

To facilitate the identification of neurons that responded to a given stimulus reproducibly, an "autocorrelation map" was calculated. For each pixel the time traces $I_a(t)$ (t = 1,…,T) of all applications $a \in \{1,\ldots, N_a\}$ of a given stimulus were concatenated into a single vector $I^*(t)$ (t = 1,…, N_aT). Autocorrelation vectors C were then calculated using time shifts that were multiples of one application period T:

$$C(n) = \frac{\sum_{t=1}^{N_aT} \left(I^*\left(t + nT \bmod N_aT\right) - \overline{I^*}\right)\left(I^*(t) - \overline{I^*}\right)}{\sum_{t=1}^{N_aT} \left(I^* - \overline{I^*}\right)^2}$$

for n = 1,…, (N_a – 1) and averaged. The result is a map that indicates positions which exhibited similar time courses during the repeated applications of the stimulus.

Determination of the Response Latencies

1. Smoothing. The Ca^{2+} trace (light blue in top panel of Figure 1B) is smoothed using the edge preserving Kuwahara filter (Kuwahara et al., 1976) with a width of 30 ms (dark blue line).
2. Approximation of latency by fitting. A function f_{fit}, consisting of a linear "baseline" followed by a double-exponential function, was fitted to the trace (green line):

$$f_{\text{fit}}(t) = \begin{cases} a_{\text{lin}} \cdot t + f_0 \\ a_{\text{lin}} \cdot t_{\text{on}}^{\text{fit}} + f_0 + a_{\text{exp}} \cdot \mathrm{e}^{-(t - t_{\text{on}}^{\text{fit}})/\tau_{\text{decay}}} \cdot \left(1 - \mathrm{e}^{-(t - t_{\text{on}}^{\text{fit}})/\tau_{\text{rise}}}\right) \end{cases} \begin{matrix} , t < t_{\text{on}}^{\text{fit}} \\ , t \geq t_{\text{on}}^{\text{fit}} \end{matrix}$$

   $(a_{\text{lin}}, a_{\text{exp}}, f_0 = f(t=0), \tau_{\text{rise}}, \tau_{\text{decay}}, \text{and } t_{\text{on}}^{\text{fit}}\,[\text{green broken line}]$ are fitting parameters.)

3. Linear regression. The onset was characterized as a significant deviation from a linear baseline in a time window ± 100 ms (gray area in Figure 1B, bottom panel) around $t_{\text{on}}^{\text{fit}}$. To this end, the linear regression f_{regr} (red line) in a moving time window of 300 ms was used to calculate linear prediction intervals (red error bars) for later time points ($f_{\text{regr}}(t_n) = a_{\text{regr}} \cdot t + b + \varepsilon$, assuming a normal distribution of the residuals $\varepsilon = N(0, \sigma^2)$, Beichelt and Montgomery, 2003). The time window was moved from early toward later times (starting at $t_{M+1} = t_{\text{on}}^{\text{fit}} - 100$ ms), until 20 consecutive data points are found outside of the prediction intervals. (The analysis was found to be insensitive to the exact number of time points.) The first of these time points was taken as the response latency (red broken line).
   Traces for which the signal-to-noise ratio was too small to determine the latency were not included in the subsequent analysis, neither were neurons that showed consistently high levels of spontaneous activity.

Response Latencies and Latency Vectors

Each slice preparation was stimulated with N_s different odors, each being presented N_a times (in randomized order). For each selected cell $c \in \{1,\ldots, N_c\}$ the response latencies were determined for each trial $a \in \{1,\ldots, N_a\}$ and stimulus $s \in \{1,\ldots, N_s\}$, resulting in a 3D matrix L(s,a,c) of response latencies. Due to missing values in this matrix (cell not responding or latency not accessible) latency vectors can have different lengths. This parameter was taken into account by using color-coded histograms and weighted means and standard deviations. The following notations are used to refer to subsets of this matrix:

- $L_S(a,c) \equiv L(s,a,c)|_{s \equiv S}$ are the latencies of all cells and trials for stimulus S.
- $L_{S,C}(a) \equiv L(s,a,c)|_{s \equiv S, c \equiv C}$ are the latencies of all trials for cell C and stimulus S.
- $L_{S,A}(c) \equiv L(s,a,c)|_{s \equiv S, a \equiv A}$ are the latencies of all cells for the A^{th} application of the stimulus S. A vector of this type is also referred to as "latency vector," as it contains the (simultaneously recorded) latencies of a population of M/T cells upon odor application.

Correlation Coefficient and Rank Correlation Coefficient

The correlation coefficient $cc_{(i,m),(j,n)}$ of a pair of latency vectors $L_{S_i,A_m}(c)$ and $L_{S_j,A_n}(c)$ (see for example Figure 2D) is given by

$$cc_{(i,m),(j,n)} = \frac{\frac{1}{N_c^*}\sum_{c=1}^{N_c^*}\left(L_{S_i,A_m}(c) - \overline{L}_{S_i,A_m}\right)\cdot\left(L_{S_j,A_n}(c) - \overline{L}_{S_j,A_n}\right)}{\sqrt{\frac{1}{N_c^*}\sum_{c=1}^{N_c^*}\left(L_{S_i,A_m}(c) - \overline{L}_{S_i,A_m}\right)^2 \cdot \left(L_{S_j,A_n}(c) - \overline{L}_{S_j,A_n}\right)^2}}.$$

When calculating weighted average values $c\tilde{c}$, the vector's length N_c^* was used as a weight:

$$c\tilde{c} = \frac{\sum_{m,n} cc_{(i,m),(j,n)} \cdot N_c^*((i,m),(j,n))}{\sum_{m,n} N_c^*((i,m),(j,n))},$$

and correspondingly for the weighted standard deviation $\tilde{\sigma}_{cc}$ of the CC.

To calculate the RCC the neurons of a slice are assigned an (arbitrary) index. For each application, the indices of the responding neurons are sorted in the order of increasing latencies, resulting in a rank latency vector (see Figure S2). The RCC $\tau_{(i,m),(j,n)}$ for a pair of rank latency vectors is then defined as

$$\tau_{(i,m),(j,n)} = 1 - 2 \cdot \frac{N^{\text{Inv}}_{(i,m),(j,n)}}{N^{\text{Inv}}_{\text{max}}(N_c^*)},$$

with N^{Inv} being the number of inversions (Weisstein, 2002) between the two rank latency vectors and $N^{\text{Inv}}_{\text{max}}(N_c^*) = N_c^* \cdot (N_c^* - 1)/2$ being the maximum number of inversions for a sequence of length N_c^*. The normalization yields a range independent of the vector's length and identical to the range of the regular correlation coefficient. The weight factor was chosen to be the maximum number of inversions $N^{\text{Inv}}_{\text{max}}$:

$$\tilde{\tau}_{(i,m),(j,n)} = 1 - \frac{\sum_{m,n} N^{\text{Inv}}_{(i,m),(j,n)}}{\sum_{m,n} N^{\text{Inv}}_{\text{max}}\left(N_c^*((i,m),(j,n))\right)},$$

which is consistent with the definition of τ in that (1) $\tilde{\tau} \in [-1,\ 1]$ and (2) if all sequences have the same length $N_c^* \equiv N_c$, $\tilde{\tau}$ is the regular average of the RCC $\tilde{\tau} = \overline{\tau}$. Similarly, a weighted standard deviation $\tilde{\sigma}_\tau$ is defined according to

$$\tilde{\sigma}_\tau = \sqrt{\frac{\sum_{m,n}\left(\tau_{(i,m),(j,n)} - \tilde{\tau}\right)^2 \cdot N^{\text{Inv}}_{\text{max}}\left(N_c^*((i,m),(j,n))\right)}{\sum_{m,n} N^{\text{Inv}}_{\text{max}}\left(N_c^*((i,m),(j,n))\right)}}.$$

Bootstrap Sampling

This method is based on resampling the data by drawing independent samples with replacement from a given dataset. After each round of sampling, the weighted mean of the sampled set is computed, and the procedure is repeated 1000 times. The resulting values are represented as histograms.

Reconstruction of Firing Rates and Quantification of Reconstruction Efficiency

Firing rates of M/T cells were reconstructed from the intensity fluctuations of the calcium indicator dye fluo-4 using the method by Yaksi and Friedrich (Yaksi and Friedrich, 2006). The data were resampled at 40 ms to achieve optimal reconstruction while retaining a good temporal resolution (Δt = 128 ms) for most data in the original publication). The reconstruction parameters were adjusted to achieve optimal results in our preparation (τ = 1 s, width of butterworth-filter: 0.5). The average of the first three data points upon response onset was then used as the instantaneous firing rate.

For the quantification of firing rate efficiency, the reconstructed firing rates (as well as the smoothened firing rate based on the simultaneously recorded spike train) were first filtered with a Gaussian with a width of 100 ms (thereby mimicking the averaging used for the instantaneous firing rate). Following the

original publication, the correlation coefficient between both traces was then calculated as a measure for reconstruction efficiency.

Classification Tests

To test whether an odor can be predicted based on the latency vector of a single trial we used a template matching algorithm. We selected one test trial at a time, and created template vectors for each stimulus from the remaining trials. The predicted stimulus, i.e., the stimulus of the template most similar to the test trial, was compared to the actual stimulus of the test trial, thus yielding a true or false prediction. The indicated vector length (see e.g., x axis in Figure 4A) is derived from the intersection of responding neurons in the test trial and the selected template.

Generating Template Vectors Using the CC

For each trial A, the latency vector $L_{s,a}(c)$ was linearly mapped into the interval [0,1] and the weighted mean position of each cell computed across all trials of stimulus S (with the length of the latency vector used as the weight).

Generating Template Vectors Using the RCC

For the classification tests using the RCC, the procedure for the CC was modified in that the latency *order* was mapped into the interval [0,1] (i.e., the neurons were distributed equidistantly in this interval).

Distance Measure to Select the Most Similar Template

The most similar template for each trial was selected by calculating the CC and RCC (for use with the CC and RCC data, respectively) between the trial and each template, and the stimulus corresponding to the template with the highest CC or RCC was chosen as the predicted stimulus. All results are based on at least 10 and 12 predictions for data from a single slice or pooled across slices, respectively. For the time-resolved classification test, only neurons with latencies in the specified time window were considered.

Classification Using Vectors of Firing Rates

For the classification tests using instantaneous firing rates, the mean rate during the first 100 ms after response onset were determined for each neuron from the reconstructed firing rates (changing the length of this interval had virtually no effect on the presented results). Since the results regarding firing rates were compared to those regarding latency vectors using the RCC, we used the same methods for the creation of templates and the selection of the nearest template.

SUPPLEMENTAL INFORMATION

Supplemental Information includes five figures and can be found with this article online at doi:10.1016/j.neuron.2010.08.005.

ACKNOWLEDGMENTS

We would like to thank R. Friedrich for providing the MATLAB code for the reconstruction of firing rates. We further thank P. Salonikidis, I. Manzini, M. Alevra, and P. Brown for reading the manuscript, and T. Nägel, J. Kowalski, H. Benseler, and W. Gräbe for expert technical support. This project was funded by the DFG Center for Molecular Physiology of the Brain (D.S.), the DFG Excellence Cluster 171 (S.J., D.S.), the Bernstein Center for Computational Neuorscience (01GQ0432 and 01GQ1005B; S.J., E.K., D.S.) and the Bernstein Focus Neurotechnology (01GQ0811 and 01GQ0810; D.S., S.J., F.W.).

Accepted: July 20, 2010
Published: September 8, 2010

REFERENCES

Abraham, N.M., Spors, H., Carleton, A., Margrie, T.W., Kuner, T., and Schaefer, A.T. (2004). Maintaining accuracy at the expense of speed: stimulus similarity defines odor discrimination time in mice. Neuron *44*, 865–876.

Bathellier, B., Buhl, D.L., Accolla, R., and Carleton, A. (2008). Dynamic ensemble odor coding in the mammalian olfactory bulb: sensory information at different timescales. Neuron *57*, 586–598.

Beichelt, F.E., and Montgomery, D.C., eds. (2003). Teubner-Taschenbuch der Stochastik, First Edition (Teubner: Wiesbaden).

Burr, D.C., and Ross, J. (1979). How does binocular delay give information about depth? Vision Res. *19*, 523–532.

Cang, J., and Isaacson, J.S. (2003). In vivo whole-cell recording of odor-evoked synaptic transmission in the rat olfactory bulb. J. Neurosci. *23*, 4108–4116.

Carey, R.M., Verhagen, J.V., Wesson, D.W., Pírez, N., and Wachowiak, M. (2009). Temporal structure of receptor neuron input to the olfactory bulb imaged in behaving rats. J. Neurophysiol. *101*, 1073–1088.

Carr, C.E., and Konishi, M. (1990). A circuit for detection of interaural time differences in the brain stem of the barn owl. J. Neurosci. *10*, 3227–3246.

Czesnik, D., Rössler, W., Kirchner, F., Gennerich, A., and Schild, D. (2003). Neuronal representation of odourants in the olfactory bulb of *Xenopus laevis* tadpoles. Eur. J. Neurosci. *17*, 113–118.

Delorme, A. (2003). Early cortical orientation selectivity: how fast inhibition decodes the order of spike latencies. J. Comput. Neurosci. *15*, 357–365.

Friedrich, R.W., and Laurent, G. (2001). Dynamic optimization of odor representations by slow temporal patterning of mitral cell activity. Science *291*, 889–894.

Gawne, T.J., Kjaer, T.W., and Richmond, B.J. (1996). Latency: another potential code for feature binding in striate cortex. J. Neurophysiol. *76*, 1356–1360.

Getchell, T.V., and Shepherd, G.M. (1978). Responses of olfactory receptor cells to step pulses of odour at different concentrations in the salamander. J. Physiol. *282*, 521–540.

Gollisch, T., and Meister, M. (2008). Rapid neural coding in the retina with relative spike latencies. Science *319*, 1108–1111.

Gomez, G., and Atema, J. (1996). Temporal resolution in olfaction: stimulus integration time of lobster chemoreceptor cells. J. Exp. Biol. *199*, 1771–1779.

Gross-Isseroff, R., and Lancet, D. (1988). Concentration-dependent changes of perceived odor quality. Chem. Senses *13*, 191–204.

Gütig, R., and Sompolinsky, H. (2006). The tempotron: a neuron that learns spike timing-based decisions. Nat. Neurosci. *9*, 420–428.

Heil, P. (1997). Auditory cortical onset responses revisited. II. Response strength. J. Neurophysiol. *77*, 2642–2660.

Hopfield, J.J. (1995). Pattern recognition computation using action potential timing for stimulus representation. Nature *376*, 33–36.

Johansson, R.S., and Birznieks, I. (2004). First spikes in ensembles of human tactile afferents code complex spatial fingertip events. Nat. Neurosci. *7*, 170–177.

Junek, S., Chen, T.W., Alevra, M., and Schild, D. (2009). Activity correlation imaging: visualizing function and structure of neuronal populations. Biophys. J. *96*, 3801–3809.

Kauer, J.S., and Shepherd, G.M. (1977). Analysis of the onset phase of olfactory bulb unit responses to odour pulses in the salamander. J. Physiol. *272*, 495–516.

Kendall, M., and Gibbons, J.D. (1990). Rank Correlation Methods, 5th edition (London: Edward Arnold, A division of Hodder & Stoughton, A Charles Griffin title)., pp. 29–50.

Khan, A.G., Thattai, M., and Bhalla, U.S. (2008). Odor representations in the rat olfactory bulb change smoothly with morphing stimuli. Neuron *57*, 571–585.

Kiseleva, E.I. (1995). Natural amino acids as effective stimuli evoking chemoreceptor-directed behavior in anuran tadpoles. Zh. Obshch. Biol. *56*, 329–345.

Kuwahara, M., Hachimura, K., Eiho, S., and Kinoshita, M. (1976). Processing of RI-angiocardiographic images. In Digital Processing of Biomedical Images (Tokyo: University of Tokyo Press), pp. 187–202.

Laing, D.G. (1986). Identification of single dissimilar odors is achieved by humans with a single sniff. Physiol. Behav. *37*, 163–170.

Laing, D.G., Eddy, A., Francis, G.W., and Stephens, L. (1994). Evidence for the temporal processing of odor mixtures in humans. Brain Res. *651*, 317–328.

Laing, D.G., Legha, P.K., Jinks, A.L., and Hutchinson, I. (2003). Relationship between molecular structure, concentration and odor qualities of oxygenated aliphatic molecules. Chem. Senses *28*, 57–69.

Lam, Y.W., Cohen, L.B., and Zochowski, M.R. (2003). Odorant specificity of three oscillations and the DC signal in the turtle olfactory bulb. Eur. J. Neurosci. *17*, 436–446.

Laurent, G., Stopfer, M., Friedrich, R.W., Rabinovich, M.I., Volkovskii, A., and Abarbanel, H.D. (2001). Odor encoding as an active, dynamical process: experiments, computation, and theory. Annu. Rev. Neurosci. *24*, 263–297.

Lehmkuhle, M.J., Normann, R.A., and Maynard, E.M. (2006). Trial-by-trial discrimination of three enantiomer pairs by neural ensembles in mammalian olfactory bulb. J. Neurophysiol. *95*, 1369–1379.

Lin, B.J., Chen, T.W., and Schild, D. (2007). Cell type-specific relationships between spiking and $[Ca^{2+}]_i$ in neurons of the *Xenopus* tadpole olfactory bulb. J. Physiol. *582*, 163–175.

Manzini, I., Peters, F., and Schild, D. (2002). Odorant responses of *Xenopus laevis* tadpole olfactory neurons: a comparison between preparations. J. Neurosci. Methods *121*, 159–167.

Manzini, I., Schweer, T.S., and Schild, D. (2008). Improved fluorescent (calcium indicator) dye uptake in brain slices by blocking multidrug resistance transporters. J. Neurosci. Methods *167*, 140–147.

Manzini, I., Heermann, S., Czesnik, D., Brase, C., Schild, D., and Rössler, W. (2007). Presynaptic protein distribution and odour mapping in glomeruli of the olfactory bulb of *Xenopus laevis* tadpoles. Eur. J. Neurosci. *26*, 925–934.

Margrie, T.W., and Schaefer, A.T. (2003). Theta oscillation coupled spike latencies yield computational vigour in a mammalian sensory system. J. Physiol. *546*, 363–374.

Moreaux, L., and Laurent, G. (2008). A simple method to reconstruct firing rates from dendritic calcium signals. Front Neurosci *2*, 176–185.

Nieuwkoop, P., and Faber, J., eds. (1967). Normal table of Xenopus laevis (Daudin), 2nd edition (New York: Garland Publishing Inc).

Panzeri, S., Petersen, R.S., Schultz, S.R., Lebedev, M., and Diamond, M.E. (2001). The role of spike timing in the coding of stimulus location in rat somatosensory cortex. Neuron *29*, 769–777.

Petersen, R.S., Panzeri, S., and Diamond, M.E. (2002). The role of individual spikes and spike patterns in population coding of stimulus location in rat somatosensory cortex. Biosystems *67*, 187–193.

Rinberg, D., Koulakov, A., and Gelperin, A. (2006). Sparse odor coding in awake behaving mice. J. Neurosci. *26*, 8857–8865.

Van Rullen, R., and Thorpe, S.J. (2001). Rate coding versus temporal order coding: what the retinal ganglion cells tell the visual cortex. Neural Comput. *13*, 1255–1283.

Schaefer, A.T., and Margrie, T.W. (2007). Spatiotemporal representations in the olfactory system. Trends Neurosci. *30*, 92–100.

Scott, J.W. (2006). Sniffing and spatiotemporal coding in olfaction. Chem. Senses *31*, 119–130.

Slotnick, B. (2007). Odor-sampling time of mice under different conditions. Chem. Senses *32*, 445–454.

Spors, H., and Grinvald, A. (2002). Spatio-temporal dynamics of odor representations in the mammalian olfactory bulb. Neuron *34*, 301–315.

Spors, H., Wachowiak, M., Cohen, L.B., and Friedrich, R.W. (2006). Temporal dynamics and latency patterns of receptor neuron input to the olfactory bulb. J. Neurosci. *26*, 1247–1259.

Thorpe, S., Delorme, A., and Van Rullen, R. (2001). Spike-based strategies for rapid processing. Neural Netw. *14*, 715–725.

Thorpe, S., and Gautrais, J. (1998). Rank order coding in CNS '97: Proceedings of the sixth annual conference on Computational neuroscience: trends in research, 1998 (New York: Plenum Press)., pp. 113–118.

Uchida, N., and Mainen, Z.F. (2003). Speed and accuracy of olfactory discrimination in the rat. Nat. Neurosci. *6*, 1224–1229.

Verhagen, J.V., Wesson, D.W., Netoff, T.I., White, J.A., and Wachowiak, M. (2007). Sniffing controls an adaptive filter of sensory input to the olfactory bulb. Nat. Neurosci. *10*, 631–639.

Weisstein, E.W. (2002). CRC Concise Encyclopedia of Mathematics, 2nd edition (Chapman & Hall / CRC).

Wellis, D.P., Scott, J.W., and Harrison, T.A. (1989). Discrimination among odorants by single neurons of the rat olfactory bulb. J. Neurophysiol. *61*, 1161–1177.

Wesson, D.W., Carey, R.M., Verhagen, J.V., and Wachowiak, M. (2008). Rapid encoding and perception of novel odors in the rat. PLoS Biol. *6*, e82.

Wesson, D.W., Verhagen, J.V., and Wachowiak, M. (2009). Why sniff fast? The relationship between sniff frequency, odor discrimination, and receptor neuron activation in the rat. J. Neurophysiol. *101*, 1089–1102.

Wright, G.A., Thomson, M.G.A., and Smith, B.H. (2005). Odour concentration affects odour identity in honeybees. Proc. Biol. Sci. *272*, 2417–2422.

Yaksi, E., and Friedrich, R.W. (2006). Reconstruction of firing rate changes across neuronal populations by temporally deconvolved Ca^{2+} imaging. Nat. Methods *3*, 377–383.